Solid State Communications 250 (2017) 9–13

Contents lists available at ScienceDirect

Solid State Communications

journal homepage: www.elsevier.com/locate/ssc

Communication

Electric field modulation of the band structure in MoS_2/WS_2 van der waals heterostructure

Wei Li[a,c], Tianxing Wang[a], Xianqi Dai[a,b,*], Xiaolong Wang[a], Caiyun Zhai[a], Yaqiang Ma[a], Shanshan Chang[a], Yanan Tang[b]

[a] College of Physics and Electronic Engineering, Henan Normal University, Xinxiang 453007, China
[b] Department of Physics, Zhengzhou Normal University, Zhengzhou, Henan 450044, China
[c] School of Mathematics & Physics, Henan University of Urban Construction, Pingdingshan 467036, China

ARTICLE INFO

Keywords:
C. MoS_2/WS_2 heterostructure
D. band structure
B. external electric field

ABSTRACT

Using density functional theory calculations, we investigate the bandstructure of MoS_2/WS_2 van der waals heterostructure by applying external electric field perpendicular to the layers. It is demonstrated that the MoS_2/WS_2 is a type-II heterostructure, and therefore the electrons and holes are spatially separated. The band gap of MoS_2/WS_2 heterostructure continuously decreases with increasing external electric field, eventually a transition from semiconductor to metal is observed. Applying external electric field along +z direction and −z directions has different effects on the band gap due to the intrinsic spontaneous polarization in MoS_2/WS_2 heterostructure. The calculated result indicates that the band inversion in MoS_2/WS_2 heterostructure can be induced by changing the strength of the external electric field. The external electric field can significantly tune the band offsets almost linearly and modify the band alignment between MoS_2 and WS_2. The present study would open a new avenue for application of such transition-metal dichalcogenides heterostructures in future nano- and optoelectronics.

1. Introduction

Despite being a very promising two-dimensional (2D) material, gapless graphene has limitation in next-generation electronic and photonic applications [1–3]. As alternatives, new research interests have emerged focusing on other 2D materials such as transition metal sulfides (TMDs), which possess sizable band gap around 1–3 eV and display advantageous optoelectronic properties [4–7]. For example, monolayer MoS_2 has a high PL quantum yield on the order of $\sim 4\times10^{-3}$ and monolayer WSe_2 is found to exhibit greater PL intensity than MoS_2 [8,9]. The single-layer MoS_2 based field-effect transistors exhibit an excellent current on/off ratio of 10^8, and the application of monolayer MoS_2 in integrated circuits and logic operations has already been realized [10,11]. For photodetection, the layered TMDs based photodetectors have been demonstrated with very high responsivity and fast photoresponse [12–14]. For the layered TMDs' applications in optoelectronics, tunable electronic properties are crucial. If the band gap can be tuned, meaning that a semiconductor with a lower band gap or a semiconductor-to-metal transition can be obtained, nanodevices with a wide range of tunable band gaps may be fabricated.

To achieve tunable electronic properties, heterostructures have been widely constructed for the conventional semiconductors. The isolation of various 2D materials in recent years [15,16] has raised the possibility of designing van der Waals (vdW) heterostructures, which provide more opportunities for achieving desired electronic or optoelectronic properties [17–19]. Since the weak van der Waals interlayer coupling is used, the lattice-matching requirement is relaxed. Thus, a huge number of combinations can be designed and explored [20]. For instance, Haigh et al. indicated the possibility of utilizing graphene-BN vertical heterostructure as an electronic device [21]. Successful synthesis of flexible and transparent memory devices consisting entirely of stacked two-dimensional materials such as graphene and MoS_2 were reported by Choi et al. [22]. In recent experiments on MoS_2-WSe_2 heterostructures, quenching of photoluminescence (PL) was observed [23], which indicates the interlayer charge transfer, and their applications in photovoltaic [24] and field effect transistors [25] were demonstrated. Recently, ultrafast hole transfer fromMoS_2 to WS_2 [26] and long lifetimes of indirect excitons in a $MoSe_2$-WSe_2 heterostructure were revealed [27]. More recent works have also demonstrated that vertical and in-plane heterostructures o MoS_2 and WS_2 can be efficiently used for light detection and Harvesting [28–30].

Though the electronic properties of graphene/BN, graphene/TMd,

* Corresponding author at: College of Physics and Electronic Engineering, Henan Normal University, Xinxiang 453007, China.
E-mail address: xqdai@htu.cn (X. Dai).

http://dx.doi.org/10.1016/j.ssc.2016.11.006
Received 23 March 2016; Accepted 3 November 2016
Available online 11 November 2016
0038-1098/

and TMD/TMD heterostructures have been studied, few reports focus on band gap tuning of TMD/TMD heterostructures using external electric field. External electric field has been recognized as one of the best possible strategies [31–42] to modulate the band gap, since it does not attenuate the properties and is remarkably simple for exploring new functionalities with a transistor configuration. by applying external electric field, features similar to nanopatterning and chemical treatment can be obtained, without permanent effect on the TMDs, as this process is fully reversible. In addition, performance and functionality of these optoelectronic devices are critically dependent on the band alignment. The most common band alignment between two different semiconductors is type-I or type-II. Considering that the band gap of layered TMDs can be effectively tuned by external electric field [43–46], one may raise the question.

whether it is possible to modify the band alignment of TMD/TMD heterostructures (e.g., from type-II to type-I) by external electric field. In this work, the electronic properties of vertical heterostructures of MoS_2 and WS_2 are investigated by using firstprinciple calculations. We reveal that the band gap and band alignment can be significantly modulated by external electric field. A transition from semiconductor to metal and the band inversion is observed. Applying external electric field along +z direction and −z directions has different effects on the band gap of due to the intrinsic spontaneous polarization in MoS_2/WS_2 heterostructure. Furthermore, the MoS_2/WS_2 heterostructure experiences a transition between type-I and type-II with an increasing −z direction external electric field.

2. Models and computational methods

With different stacking conformations, MoS_2 monolayer and WS_2 monolayer can form four different heterobilayer structures, which are depicted in Fig. 1: AA, C7, C27, and T stacking. First-principles calculations are performed within the framework of plane-wave density functional theory, implemented in the Vienna ab initio simulation package (VASP) [47,48]. The generalized gradient approximation of Perdew, Burke, andErnzerhof (GGA-PBE) [49] with van der Waals (vdW) correction proposed by Grimme (DFT-D2) [50] is chosen due to its good description of long-range vdW interactions [51–56]. The energy cutoff in calculations was set to be 500 eV, and the total energy was converged to better than 10^{-5} eV. The equilibrium structures were obtained through structural relaxation until Hellmann–Feynman forces were less than 0.01 eV/Å. The 2D Brillouin zone integration using the Γ-center scheme is sampled with a 9×9×1 grid for geometry optimization and a 15×15×1 grid for static electronic structure calculations. All calculations are carried out using a 1×1 supercell. The vacuum size is larger than 20 Å between two adjacent images to prevent spurious interactions between periodic images of the slabs.

Table 1
Total energies (denoted as Etot) of MoS_2/WS_2 heterostructure with four stacking conformations.

Stacking	AA	C7	C27	T
Etot(eV)	0.048	0.000	0.012	0.003

3. Results and discussion

3.1. Geometries, stabilities, and band structures of of MoS_2/WS_2 heterostructure

The total energies (denoted as Etot) of four different heterobilayer structures are given in Table 1. The energies listed in Table 1 are relative to the Etot of C7 stacking. From Table 1, it can be concluded that, among the different heterobilayer structures considered here, the most stable heterobilayer structure is C7 stacking. In the following, only the C7 stacking is considered. The interlayer distance d (Fig. 1) and the binding energy per unit cell of MoS_2/WS_2 heterostructure are calculated to determine the interaction between MoS_2 and WS_2 layer. The binding energy are defined as

$$E_b = E_{total} - E_{MoS_2} - E_{WS_2},$$

where E_{total}, $E_{MoS_2}$and E_{WS_2} are the energies of the MoS_2/WS_2 heterostructure, the freestanding MoS_2 and WS_2 monolayer, respectively. The calculated interlayer distance(3.258 Å) is much larger than the sum of the covalent radii of the S and S atoms, which means that the S atoms of MoS_2 and the S atoms of WS_2 are beyond the bonding range. The binding energy of MoS_2/WS_2 heterostructure is −0.226 eV, further supporting the weak van der Waals interaction between the MoS_2 and WS_2 layers.

The band structures of monolayers as well as the projected band structure of MoS_2/WS_2 heterostructure are given in Fig. 2. In the projected band structure of MoS_2/WS_2 heterostructure, the bands dominated by MoS_2 and WS_2 are plotted by red and blue circles, respectively. As shown in Fig. 2, the electronic structures of both the MoS_2 and the WS_2 layers are well-preserved. The MoS_2 and the WS_2 monolayers are direct semiconductors with the conduction band minimum (CBM) and valence band maximum (VBM) being located at the K point. MoS_2/WS_2 is an indirect semiconductor, which possess an indirect band gap of 1.4355 eV. Different from their homogeneous bilayers, the CBM of MoS_2/WS_2 is located at the K point, while the VBM is located at the Γ point. As can be seen from Fig. 2, the CBM and VBM of MoS_2/WS_2 heterostructure are strictly localized to one of the

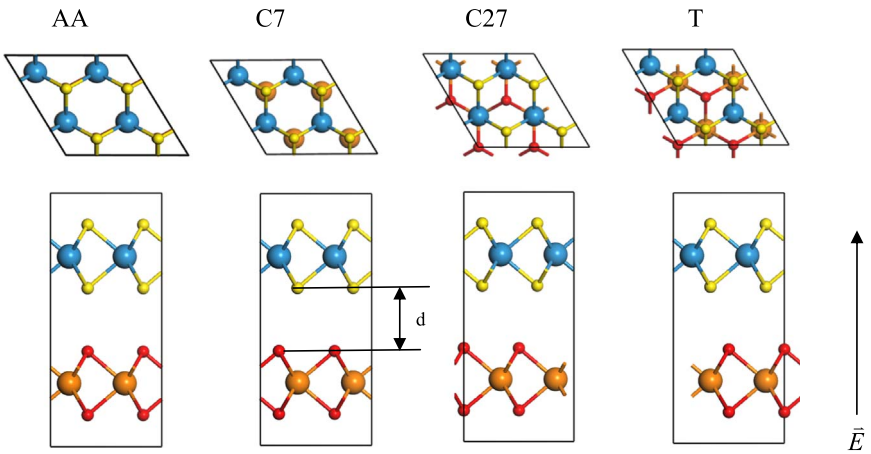

Fig. 1. Top (upper panel) and side (lower panel) views of the MoS_2/WS_2 heterostructure with four different types of layer-on-layer stacking. The Mo, W, S in the MoS_2 layer and S in the WS_2 layer are represented by orange, blue, red and yellow spheres, respectively. The arrow indicates the positive direction of the external electric field, pointing from MoS_2 to WS_2.

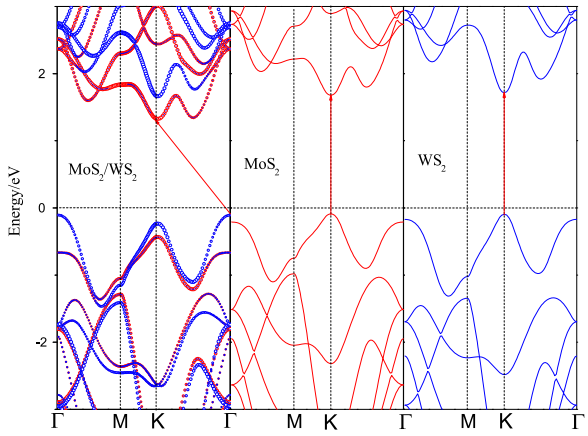

Fig. 2. Band structures of monolayer MoS_2, WS_2, and MoS_2/WS_2 heterostructure. Projection to MoS_2 layer is denoted by red circles and to WS_2 by blue circles. The Fermi level is set as zero.

monolayers: CBM is completely localized to MoS_2 and VBM to WS_2. The monolayer MoS_2 and monolayer WS_2 form an atomically sharp type-II heterointerface through van der Waals interaction, which may be of advantageous for the separation of electron–hole pairs. In a type-II heterostructure, free electrons and holes will be spontaneously separated, which is suitable for optoelectronics and solar energy conversion.

3.2. *Effect of external electric field to the band gap of MoS_2/WS_2 heterostructure*

Previous studies indicate that a band gap can be modulated by a vertical applied electric field in bilayer TMDCs, and the semiconductor-to-metal transition occurs when the electric field is further increased [57–59]. Will the external electric field induce the semiconductor-to-metal transition in MoS_2/WS_2 heterostructure? Our test calculation shows that the answer to this question is yes. We apply an external electric field on the MoS_2/WS_2 heterostructure. The external electric field is vertical to the basal planes of MoS_2/WS_2 heterostructure. An overview of the band structures of MoS_2/WS_2 as a function of external electric field is elucidated in Fig. 3. It is apparent at a glance that the band gap is driven continuously to zero with increasing external electric fields. It is found that the fundamental band gap without an external electric field is an indirec gap between the VBM at Γ and CBM at K. The external electric field shifts the VBM to the K point. The system still has an indirect band-gap when the electric field is less than

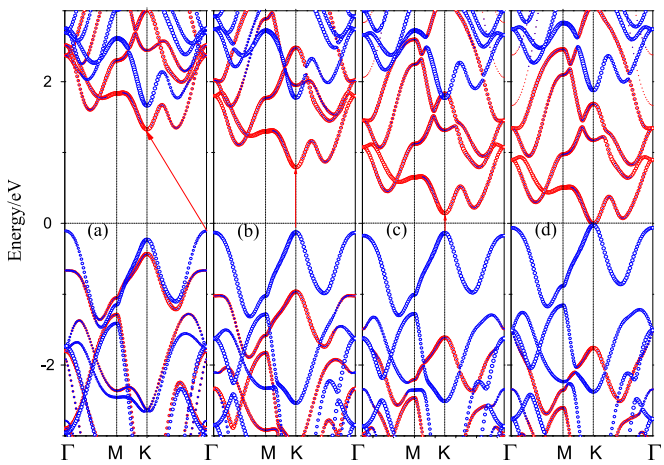

Fig. 3. Band structures of MoS_2/WS_2 heterostructure under E_{ext}=0 V/nm(a), E_{ext}=1 V/nm(b), E_{ext}=2 V/nm(c) and E_{ext}=2.4 V/nm(d). Projection to MoS_2 layer is denoted by red circles and to WS_2 by blue circles. The Fermi level is set as zero.

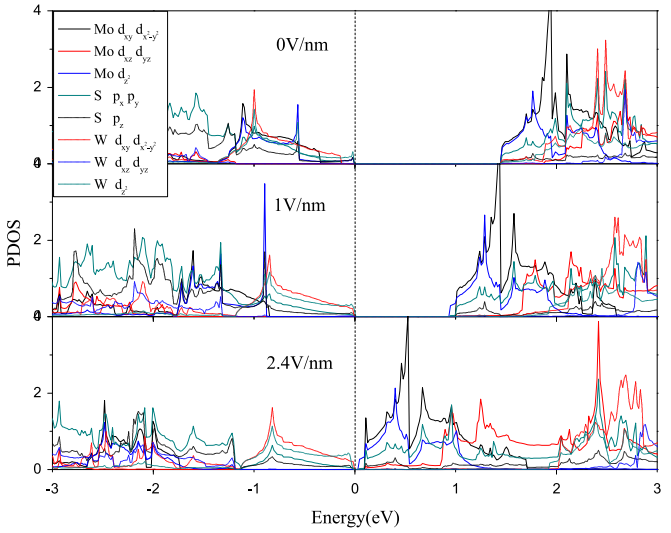

Fig. 4. Partial density of states (PDOS) as a function of applied external electric field for MoS_2/WS_2 heterostructure.

1 V/nm. Once the external electric field approaches 1 V/nm, the indirect band gap of the heterostructure transforms to a direct band gap with VBM and CBM locating at the K point as shown in Fig. 3(*b*). When the external electric field is above 1 V/nm, the heterostructure retains the direct band-gap feature (Fig. 3(*c*) and (*d*)), and gap closing occurs at the K point with increasing external electric fields. The calculated results indicate that the external electric field is an effective strategy to tune the band gap of MoS_2/WS_2.

To attain more insight into the physical mechanisms underlying the band gap modulation by the electric field, a more detailed electronic structure analysis is performed. The partial density of states (PDOS) as a function of external electric field for MoS_2/WS_2 heterostructure is shown in Fig. 4. The indirect band gap of MoS_2/WS_2 heterostructure is determined by the Γ point energy level and the K point energy level without an external elcetric field. The VBM (Γ point) is composed primarily of W-d_z^2 states and p_z orbitals from S atoms in the WS_2 layer. Due to the presence of vacuum, these p_z orbitals do not interact with antibonding orbitals on S atoms from the neighboring layer; thus the states are lower in energy and make smaller contributions to VBM. The CBM (K point) is mainly described by Mo- dz^2 orbital. The external electric field results in upward shifting of the valence band around K point, but does not affect the valence band around Γ point. This causes a shift in VBM from Γ point to K point, which is mainly described by S p_x-p_y, p_z and W dxy-dx^2-y^2, dz^2 orbitals. Upon application of an external electric field, the CBM is still at K point, which is mainly described by S p_x-p_y, p_z and Mo dxy-dx^2-y^2, dz^2 orbitals. That leads to indirect-to-direct band gap transformation at 1 V/nm. The electrostatic energy felt by an electron in WS_2 layer becomes higher and that in MoS_2 layer becomes lower. This makes the band energy of electrons in WS_2 layer rise and lower in MoS_2 layer. Moving of energy bands in opposite direction results in the decrease of band gap. Consequently, depending on the strength of external electric field, the band gap of MoS_2/WS_2 heterostructure can be effectively and continuously tuned, and the semiconductor–metal transition can be achieved.

Evolution of the band gap as a function of the external electric field is given in Fig. 5. The band gap of the heterostructure decreases almost linearly to the external vertical electric field because of the giant Stark effect, eventually achieving a semiconductor-metal transition at the critical external electric field. However, the response of the band gap to positive and negative fields (the direction defined in Fig. 1) is distinct. This is because in MoS_2/WS_2 heterostructure dose the intrinsic spontaneous polarization exist, the intrinsic spontaneous polarization may stem from the electronegativity difference between Mo and W.

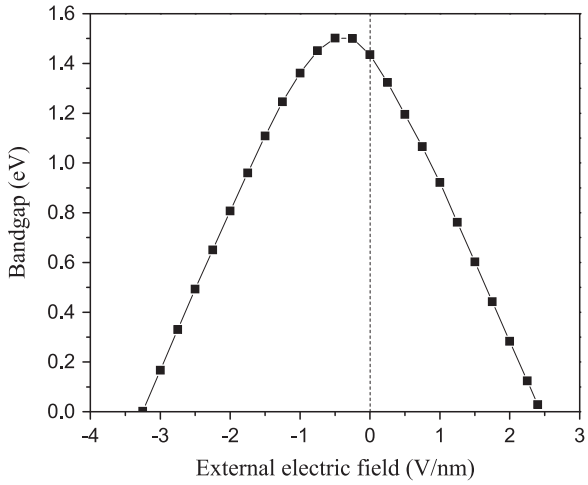

Fig. 5. Band gap of MoS_2/WS_2 heterostructure as a function of external electric field along +z and −z directions.

Under a positive external electric field, the band gap of the heterostructure continuously decreases with increasing external electric field and achieves zero at 2.4 V/nm, which shares the same qualitative trend with the homogeneous bilayer structures. While, the critical external electric field is smaller than that of bilayer MoS_2 (3 V/nm) and bilayer WS_2 (2.7 V/nm) [59] due to the presence of the intrinsic spontaneous polarization, which has a superimposing effect with the external electric field. This indicates that the MoS_2/WS_2 heterostructure is more responsive to tuning by an external electric field than MoS_2 and WS_2 homogeneous bilayer structures. The S atoms of the top monolayer and the Mo atoms of the bottom monolayer are superimposed, meanwhile the W atoms of the top monolayer and the S atoms of the bottom monolayer are also superimposed. The electronegativity of Mo and W are different, so there exists a spontaneous electrical polarization along the +z direction. Opposite to the linear decrease under a positive external electric field, the band gap first increases until −0.5 V/nm, reaching up to 1.50 eV, but then, it decreases linearly and eventually turns metallic at −3.3 V/nm under a negative external electric field. The initial increase of the band gap stems from the gradual neutralization of the intrinsic spontaneous polarization of MoS_2/WS_2 heterostructure. The critical electric fields of MoS_2/WS_2 heterostructure are 2.4 V/nm and 3.3 V/nm for the +z and −z direction external electric field, respectively. The critical electric field for the +z direction is smaller than that of −z direction due to the presence of the intrinsic spontaneous polarization along the +z direction, it has a shift of 0.5 V/nm along the −z direction.

3.3. Band inversion and tunable band offsets in MoS_2/WS_2 heterostructure

More interestingly, once the critical external electric field approaches 2.4 V/nm, the band gap at the K point is driven rapidly to zero and then is incremental with negative values, i.e., the conduction band and the valence band around the Fermi level are inverted, which indicates band inversion characterizations. The projected band structures of MoS_2/WS_2 under an external elcetric field of 2.7 V/nm are depicted in Fig. 6. The band inversion characterization appears at the K point yielded by the lowering of the conduction band and the rising of the valence band at the K point. From Fig. 3, we can clearly see that, below the critical external electric field of 2.4 V/nm, the main projections of the conduction band and the valence band of MoS_2/WS_2 at the K point are predominated by MoS_2 and WS_2, respectively. When the external elcetric field exceeds the critical external electric field of 2.4 V/nm, the main projections of the conduction band and the valence band of MoS_2/WS_2 at the K point are contributed by WS_2 and MoS_2,

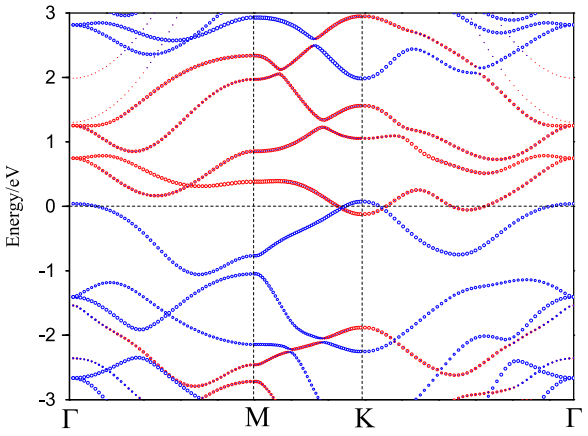

Fig. 6. The projected band structure of MoS_2/WS_2 heterostructure under an an external elcetric field of 2.7 V/nm.

respectively, meaning that band inversion at the K point takes place upon the critical external electric field. Our result indicates that the band inversion in MoS_2/WS_2 heterostructure can be induced by changing the strength of the external electric field.

In comparison with its band gap, the band offsets of MoS_2/WS_2 heterostructure is more important in logic circuits and photonic devices. The band offsets of MoS_2/WS_2 heterostructure under various external electric fields are calculated and shown in Fig. 7(a). The valence and conduction band offsets are defined as $\Delta E_V = E_{V\text{-}Mo} - E_{V\text{-}W}$ and $\Delta E_C = E_{C\text{-}Mo} - E_{C\text{-}W}$. $E_{V\text{-}Mo(W)}$ and $E_{C\text{-}Mo(W)}$ are the VBM and CBM of MoS_2 (WS_2) in MoS_2/WS_2 heterostructure, respectively. Both ΔE_V and ΔE_C indicate similar variation trend and decrease linearly with the external electric field, as shown in Fig. 7(a). In order to understand the band offsets modulation by the external electric field, the band edges of MoS_2 and WS_2 under various external electric field are calculated and shown in Fig. 7(b). As can be seen from Fig. 7(b), the VBM and CBM of WS_2 increase linearly with external electric field, while the VBM and CBM of MoS_2 show a linear decrease. The external electric field exerts little influence on the respective band gap of MoS_2 and WS_2. The MoS_2/WS_2 heterostructure experiences a transition from type-II to type-I when external electric field is −0.25 V/nm, resulting in both the VBM and CBM are localized on MoS_2. once external electric field exceeds −0.5 V/nm, the type-I heterostructure transforms to type-II with the VBM and CBM lie in MoS_2 and WS_2, respectively, which can be carefully confirmed in Fig. 7(b).

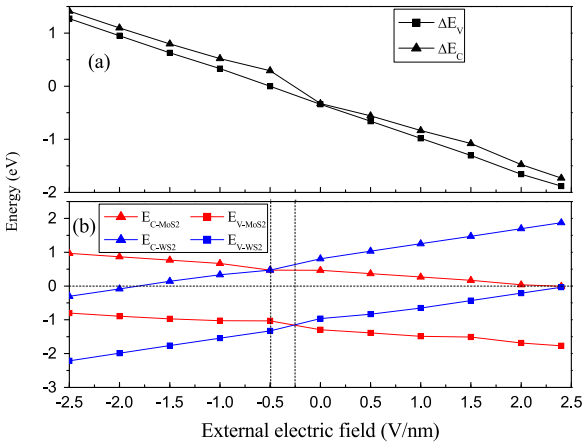

Fig. 7. (a) Evolution of the band offsets of MoS_2/WS_2 heterostructure as a function of the external electric field. (b) Evolution of the band edges of MoS_2 and WS_2 in MoS_2/WS_2 heterostructure as a function of the external electric field. $E_{V\text{-}Mo(W)}$ and $E_{C\text{-}Mo(W)}$ are the VBM and CBM of MoS_2 (WS_2) in MoS_2/WS_2 heterostructure.

4. Conclusions

In summary, by means of density functional theory computations, we have investigated the bandstructure of MoS_2/WS_2 van der waals heterostructure by applying external electric field perpendicular to the layers. Our calculations indicate that the CBM of MoS_2/WS_2 is dominated by the MoS_2 layer and the VBM by the WS_2 layer, forming a type-II heterostructure through van der Waals interaction. The type-II band alignment can facilitate the separation of electrons and holes, enabling the high efficiency of optoelectronics and solar energy conversion. The band gap of MoS_2/WS_2 heterostructure continuously decreases with increasing external electric field, eventually rendering it metallic. The response of the band gap to positive and negative fields is distinct due to the intrinsic spontaneous polarization in MoS_2/WS_2 heterostructure. The MoS_2/WS_2 heterostructure is more responsive to tuning by an external electric field than MoS_2 and WS_2 homogeneous bilayer structures. More interestingly, when external elcetric field is above the critical external electric field of 2.4 V/nm, the band inversion in MoS_2/WS_2 heterostructure can be induced. The band offsets can be significantly modulated by external electric field and change almost linearly with external electric field. Furthermore, the MoS_2/WS_2 heterostructure experiences a transition between type-I and type-II with an increasing −z direction external electric field. Our work is expected to promote the applications of such transition-metal dichalcogenides heterostructure in future nanoelectronics, photovoltaic cell, photodetector, and logical devices.

Acknowledgements

We acknowledge support from the National Natural Science Foundation of China (Grant Nos. 11504092, U1404109 and 11504334) and the High Performance Computing Center of Henan Normal University.

References

[1] A.K. Geim, Science 324 (2009) 1530.
[2] P. Avouris, Z. Chen, V. Perebeinos, Nat. Nanotechnol. 2 (2007) 605.
[3] F. Schwierz, Nat. Nanotechnol. 5 (2010) 487.
[4] D.-S. Tsai, K.L. Keng, L. Der-Hsien, L.T. Meng, F.K. Chen, A.L. Chin, J.L. Lain, H. Jr-Hau, ACS Nano 7 (2013) 3905..
[5] O. Lopez-Sanchez, L. Dominik, K. Metin, R. Aleksandra, K. Andras, Nat. Nanotechnol. 8 (2013) 497.
[6] J.N. Coleman, Science 331 (2011) 568.
[7] T. Korn, S. Heydrich, M. Hirmer, J. Schmutzler, C. Schüller, Appl. Phys. Lett. 99 (2011) 102109.
[8] K.F. Mak, C. Lee, J. Hone, J. Shan, T.F. Heinz, Phys. Rev. Lett. 105 (2010) 136805.
[9] P. Tonndorf, R. Schmidt, P. B€ottger, X. Zhang, J. B€orner, A. Liebig, M. Albrecht, C. Kloc, O. Gordan, D.R.T. Zahn, S. Michaelis de Vasconcellos, R. Bratschitsch, Opt. Express 21 (2013) 4908.
[10] B. Radisavljevic, A. Radenovic, J. Brivio, V. Giacometti, A. Kis, Nat. Nanotechnol. 6 (2011) 147.
[11] B. Radisavljevic, M.B. Whitwick, A. Kis, ACS Nano 5 (2011) 9934.
[12] D.S. Tsai, K.K. Liu, D.H. Lien, M.L. Tsai, C.F. Kang, C.A. Lin, L.J. Li, J.H. He, ACS Nano 7 (2013) 3905.
[13] O. Lopez-Sanchez, D. Lembke, M. Kayci, A. Radenovic, A. Kis, Nat. Nanotechnol. 8 (2013) 497.
[14] W. Zhang, J.-K. Huang, C.-H. Chen, Y.-H. Chang, Y.-J. Cheng, L.-J. Li, Adv. Mater. 25 (2013) 3456.
[15] J.N. Coleman, M. Lotya, A. Oeill, S.D. Bergin, P.J. King, U. Khan, K. Young, A. Gaucher, S. De, R.J. Smith, I.V. Shvets, S.K. Arora, G. Stanton, H.Y. Kim, K. Lee, G.T. Kim, G.S. Duesberg, T. Hallam, J.J. Boland, J.J. Wang, J.F. Donegan, J.C. Grunlan, G. Moriarty, A. Shmeliov, R.J. Nicholls, J.M. Perkins, E.M. Grieveson, Koenraad Theuwissen,5, David W. McComb, P.D. Nellist, V. Nicolosi, Science 331 (2011) 568.
[16] Z. Zeng, Z. Yin, X. Huang, H. Li, Q. He, G. Lu, F. Boey, H. Zhang, Angew. Chem. Int. Ed. 50 (2011) 11093.
[17] H. Fang, C. Battaglia, C. Carraro, S. Nemask, B. Ozdol, J.S. Kang, H.A. Bechtel, S.B. Desai, F. Kronast, A.A. Unal, G. Conti, C. Conlon, G.K. Palsson, M.C. Martin, A.M. Minor, C.S. Fadley, E. Yablonovitch, R. Maboudian, A. Javey, Proc. Natl. Acad. Sci. USA 111 (2014) 6198.
[18] H.P. Komsa, A.V. Krasheninnikov, Phys. Rev. B 88 (2013) 085318.
[19] J. Kang, J.B. Li, S.S. Li, J.B. Xia, L.W. Wang, Nano Lett. 13 (2013) 5485.
[20] S. Chuang, R. Kapadia, H. Fang, T.C. Chang, W.C. Yen, Y.L. Chueh, Appl. Phys. Lett. 102 (2013) 242101.
[21] S.J. Haigh, A. Gholinia, R. Jalil, S. Romani, L. Britnell, D.C. Elias, K.S. Novoselov, L.A. Ponomarenko, A.K. Geim, R. Gorbachev, Nat. Mater. 11 (2012) 764.
[22] M.S. Choi, G.-H. Lee, Y.-J. Yu, D.-Y. Lee, S.H. Lee, P. Kim, J. Hone, W.J. Yoo, Nat. Commun. 4 (2013) 1624.
[23] H. Fang, C. Battaglia, C. Carraro, S. Nemsak, B. Ozdol, J.S. Kang, H.A. Bechtel, S.B. Desai, F. Kronast, A.A. Unal, Proc. Natl. Acad. Sci. USA 111 (2014) 6198.
[24] M.M. Furchi, A. Pospischil, F. Libisch, J. Burgdorfer, T. Mueller, Nano Lett. 14 (2014) 4785.
[25] T. Roy, M. Tosun, J.S. Kang, A.B. Sachid, S.B. Desai, M. Hettick, C.C. Hu, A. Javey, ACS Nano 8 (2014) 6259.
[26] X. Hong, J. Kim, S.F. Shi, Y. Zhang, C. Jin, Y. Sun, S. Tongay, J. Wu, Y. Zhang, F. Wang, Nat. Nanotechnol. 9 (2014) 682.
[27] P. Rivera, J.R. Schaibley, A.M. Jones, J.S. Ross, S. Wu, G. Aivazian, P. Klement, N.J. Ghimire, J. Yan, D.G. Mandrus, Preprint 1403 (2014) 4985.
[28] Y. Gong, J. Lin, X. Wang, G. Shi, S. Lei, Z. Lin, X. Zou, G. Ye, R. Vajtai, B.I. Yakobson, H. Terrones, M. Terrones, B.K. Tay, J. Lou, S.T. Pantelides, Z. Liu, W. Zhou, P.M. Ajayan, Nat. Mater. 13 (2014) 1135.
[29] X. Hong, J. Kim, S.F. Shi, Y. Zhang, C. Jin, Y. Sun, S. Tongay, J. Wu, Y. Zhang, F. Wang, Nat. Nanotechnol. (9) (2014) 682.
[30] S. Tongay, W. Fan, J. Kang, J. Park, U. Koldemir, J. Suh, D.S. Narang, K. Liu, J. Ji, J. Li, R. Sinclair, J. Wu, Nano Lett. 14 (2014) 3185.
[31] K. Ueno, S. Nakamura, H. Shimotani, A. Ohtomo, N. Kimura, T. Nojima, H. Aoki, Y. Iwasa, M. Kawasaki, Nat. Mater. 7 (2008) 855.
[32] H.T. Yuan, H. Shimotani, A. Tsukazaki, A. Ohtomo, M. Kawasaki, Y. Iwasa, Adv. Funct. Mater. 19 (2009) 1046.
[33] K. Ueno, S. Nakamura, H. Shimotani, H.T. Yuan, N. Kimura, T. Nojima, H. Aoki, Y. Iwasa, M. Kawasaki, Nat. Nanotechnol. 6 (2011) 408.
[34] Y. Yamada, K. Ueno, T. Fukumura, H.T. Yuan, H. Shimotani, Y. Iwasa, L. Gu, S. Tsukimoto, Y. Ikuhara, M. Kawasaki, Science 332 (2011) 1065.
[35] K. Ueno, H. Shimotani, H.T. Yuan, J.T. Ye, M. Kawasaki, Y. Iwasa, J. Phys. Soc. Jpn. 83 (2014) 032001.
[36] H.T. Yuan, M.S. Bahramy, K. Morimoto, S.F. Wu, K. Nomura, B.J. Yang, H. Shimotani, R. Suzuki, M. Toh, C. Kloc, X.D. Xu, R. Arita, N. Nagaosa, Y. Iwasa, Nat. Phys 9 (2013) 563.
[37] Y.J. Zhang, J.T. Ye, Y. Matsuhashi, Y. Iwasa, Nano Lett. 12 (2012) 1136.
[38] Y.J. Zhang, J.T. Ye, Y. Yornogida, T. Takenobu, Y. Iwasa, Nano Lett. 13 (2013) 3023.
[39] D. Braga, I. Guti_errez Lezama, H. Berger, A.F. Morpurgo, Nano Lett. 12 (2012) 5218.
[40] J.T. Ye, Y.J. Zhang, R. Akashi, M.S. Bahramy, R. Arita, Y. Iwasa, Science 338 (2012) 1193.
[41] T.P. Kaloni, M. Tahir, U. Schwingenschl€ogl, Sci. Rep. 3 (2013) 3192.
[42] T.P. Kaloni, G. Schreckenbach, M.S. Freund, J. Phys. Chem. C 118 (2014) 23361.
[43] D. Kapildeb, D.P. Chaitanya, S. Stefano, ACS Nano 6 (2012) 4823.
[44] Q.H. Liu, L.Z. Li, Y.F. Li, Z.X. Gao, Z.F. Chen, J. Lu, J. Phys. Chem. C 116 (2012) 21556.
[45] L.Z. Kou, C. Tang, Y. Zhang, T. Heine, C.F. Chen, T. Frauenheim, J. Phys. Chem. Lett. 3 (2012) 2934.
[46] J.S. Qi, X. Li, X.F. Qian, J. Feng, Appl. Phys. Lett. 102 (2013) 173112.
[47] G. Kresse, J. Furthm¨uller, Phys. Rev. B 54 (1996) 11169.
[48] G. Kresse, J. Furthm¨uller, Comput. Mater. Sci. 6 (1996) 15.
[49] J.P. Perdew, K. Burke, M. Ernzerhof, Phys. Rev. Lett 77 (1996) 3865.
[50] S. Grimme, J. Comput. Chem 27 (2006) 1787.
[51] S. Grimme, C. Muck-Lichtenfeld, J. Antony, J. Phys. Chem. C 111 (2007) 11199.
[52] J. Antony, S. Grimme, Phys. Chem. Chem. Phys 10 (2008) 2722.
[53] N. Kharche, S.K. Nayak, Nano Lett. 11 (2011) 5274.
[54] J. Sawin′ska, P. Dabrowski, I. Zasada, Phys. Rev. B 83 (2011) 245429.
[55] R. Kagimura, M.S.C. Mazzoni, H. Chacham, Phys. Rev. B 85 (2012) 125415.
[56] Y. Ma, Y. Dai, M. Guo, B. Huang, Phys. Rev. B 85 (2012) 235448.
[57] X.Q. Dai, W. Li, T.X. Wang, X.L. Wang, C.Y. Zhai, J. Appl. Phys. 117 (2015) 084310.
[58] Q.H. Liu, L.Z. Li, Y.F. Li, Z.X. Gao, Z.F. Chen, J. Lu, J. Phys. Chem. C 116 (2012) 21556.
[59] A. Ramasubramaniam, D. Naveh, E. Towe, Phys. Rev. B 84 (2011) 205325.